gases

MDPI

Article

Computational Fluid Dynamics Analysis of a Hollow Fiber Membrane Module for Binary Gas Mixture

Salman Qadir [1,2,*], Muhammad Ahsan [1] and Arshad Hussain [3]

[1] School of Chemical and Materials Engineering (SCME), National University of Sciences and Technology, NUST, Sector H-12, Islamabad 44000, Pakistan
[2] National Energy Laboratory Dalian, Dalian Institute of Chemical Physics, Chinese Academy of Sciences, Dalian 116023, China
[3] Department of Chemical, Mechanical, Materials, and Mining Engineering, Pak-Austria Fachhochschule: Institute of Applied Sciences and Technology, Haripur 22620, Pakistan
* Correspondence: salmanqadir789@gmail.com or salman.qadir@kaust.edu.sa

Abstract: The membrane gas separation process has gained significant attention using the computational fluid dynamics (CFD) technique. This study considered the CFD method to find gas concentration profiles in a hollow fiber membrane (HFM) module to separate the binary gas mixture. The membrane was considered with a fiber thickness where each component's mass fluxes could be obtained based on the local partial pressures, solubility, diffusion, and the membrane's selectivity. COMSOL Multiphysics was used to solve the numerical solution at corresponding operating conditions and results were compared to experimental data. The two different mixtures, CO_2/CH_4 and N_2/O_2, were investigated to obtain concentration gradient and mass flux profiles of CO_2 and O_2 species in an axial direction. This study allows assessing the feed pressure's impact on the HFM system's overall performance. These results demonstrate that the increment in feed pressures decreased the membrane system's separation performance. The impact of hollow fiber length indicates that increasing the active fiber length has a higher effective mass transfer region but dilutes the permeate-side purities of O_2 (46% to 28%) and CO_2 (93% to 73%). The results show that increasing inlet pressure and a higher concentration gradient resulted in higher flux through the membrane.

Keywords: computational fluid dynamics; gas separation; hollow fiber membrane; finite element method; module design

Citation: Qadir, S.; Ahsan, M.; Hussain, A. Computational Fluid Dynamics Analysis of a Hollow Fiber Membrane Module for Binary Gas Mixture. *Gases* **2023**, *3*, 77–91. https://doi.org/10.3390/gases3020005

Academic Editors: Faizan Ahmad and Asim Khan

Received: 12 December 2022
Revised: 18 April 2023
Accepted: 5 May 2023
Published: 22 May 2023

1. Introduction

Membrane gas separation is a predominant unit operation compared to other gas separation techniques, such as distillation, adsorption, and absorption [1,2]. The membrane process is more feasible because of its smooth operation, low cost, reliability, small heat effects, and higher separation performance [3]. These advantages enhance its utilization in various industrial gas applications. Numerical methods can be used to simulate the membrane modules for process optimization [4]. Various gas separation applications deal with a gaseous mixture, such as methane recovery from carbon dioxide, nitrogen recovery from air, and helium recovery from methane [5]. The membrane module configuration is vital for gas separation performance [6]. Gas separation units are primarily applied in offshore systems because they take less space for installation [7]. The utilization of membrane separation processes for gaseous mixtures could be widely increased in 2030 [8,9].

Membrane gas separation can eliminate specific components because it is highly selective for one component to pass through it, while other components are retained at the feed side [1,10]. It is a traditional process because of its high membrane selectivity, low maintenance cost, and simple unit operation [11–13]. Due to high market demand, the membranes are used for commercial applications to separate gaseous mixtures and are less economical [14,15]. Membrane gas separation has many applications such as

hydrogen recovery in refineries, sour gas treatment, hydrogen recovery from ammonia, air separation for oxygen purification, and carbon dioxide removal from natural for large scale [16]. In heavy oil and petrochemical industries, membrane systems have integrated with other industrial units, but the scenarios for different groups are limitless. The growth of membrane systems for gaseous mixture separation was estimated to increase widely in 2023 [8,17]. Therefore, this technology will reduce the overall process cost for gas separation and environmental impacts [18].

Numerical approaches can solve gas separation through membrane flow difficulties to improve the configuration [19]. In addition, numerical methods have predicted values at various mesh edges for different flow conditions and given more precise results [20]. Mathematical modeling is a time- and cost-saving approach for unnecessary experimental designs [21]. Therefore, CFD modeling is used for investigating the flow problems across the membrane surface [22]. CFD techniques are applied to understand the phenomena inside the membrane and the separation performance of different membrane modules [17]. CFD allows changing the parameters for different gases obtained from the concentration profiles [23]. The CFD tool is mostly applied to visualize the membrane module's fluid hydrodynamics and flow patterns on permeate and retentate streams [9,15]. It is critical because different hydrodynamic conditions affect the transport mechanism [24]. Membrane module design is also essential for improving the efficiency of gas permeation performance through the membrane [25]. The CFD technique has been used for flow behavior in the rectangular channel with different feed spacers [16,26]. Many researchers have studied the flow characteristics of membrane modules for gas separation processes.

The properties of membrane materials for designing industrial module and process design play an essential role in successfully implementing the gas separation system [27]. For industrial applications, the HFM module's design depends on the module's cost and efficiency. Therefore, the HFM module requires a maximum membrane surface area for separation, which is necessary to determine the concentration profiles and pressure drops along with the module length [24,28]. In recent studies, the asymmetric hollow fiber membrane configuration was used for gas separation, demonstrating higher flux [10]. The counter-current flow pattern investigated the process effect on different design variables [29,30]. A three-dimensional membrane model was developed considering a non-isothermal model for evaluating temperature's effect on membrane permeance [31]. The CFD technique was used for a perovskite HFM to investigate the oxygen permeation through the membrane. It showed the effect of pressure on permeate streams in the range of 0.2 to 0.4 kPa, and different vacuum levels were used to obtain the oxygen concentration profile at the feed side [32].

The HFM module separates binary gas using this research work's finite element method (COMSOL Multiphysics simulation software). Three-dimensional geometry was developed for the separation of the binary gas mixture. The CFD tool was applied to study the flow profiles of gases in the HFM membrane module. Two binary mixture systems, N_2/O_2 and CO_2/CH_4, were investigated. In this study, different membrane module parameters, fiber length (L), inlet pressure (pf), inlet concentration (xf), fiber bundle radius (Ro), and module outer diameter (Do), were optimized. Lastly, gas separation through membrane modules was studied with different module parametric effects.

2. Materials and Methods

CFD deals with partial differential equations based on mass, momentum, and heat transport. The CFD technique is used for simulating different integrated parts of industrial HFM units. Therefore, the HFM membrane module is used to understand gas separation phenomena. Table 1 shows the parameters used for simulations. A numerical simulation was carried out using the COMSOL Multiphysics® package. The 3-Dimensional geometries of the HFM module were developed in axisymmetric model. The transport of diluted species with Fick's Law model was considered for transport through the membrane. The following assumptions was required for this model.

Table 1. Properties for HFM module.

Parameters	Symbols	Hollow Fiber Membrane Module [33–37]		Units
Inlet pressure	pf	790.8	6895	Pa
Permeate pressure	ph	101.3	138	Pa
Inlet gas	C_0	0.205 O_2	0.5 CO_2	Mole fraction
Permeance	P	30.78×10^{-10}	33×10^{-10}	mol/m^2. s.pa
Module diameter	Do	9.5×10^{-3}	20×10^{-3}	m
Module length	L	0.25	0.1	m
Membrane thickness	δ	0.08	0.0004	mm

2.1. Assumptions

The following assumptions were used for the modeling of the HFM membrane module: [38,39]

a. Steady-state condition is applied.
b. Laminar flow is considered with constant physical properties.
c. Ideal gas law is used.
d. Without axial mixing of gaseous molecules.
e. Fiber diameter in the module is uniform.
f. Fiber deformation with high inlet pressure is neglected.
g. Solution-diffusion mechanism is used for membrane gas separation.

2.2. Mass Transport Mathematical Modeling

In the mass transport phenomena, chemical species are transferred through the membrane from the shell to the permeate. The mass transport of components has occurred due to the concentration difference from the feed side to permeate side through the membrane using diffusion and the molecular sieving mechanism shown in the Figure 1. In this model, the convective mass transport occurs with a different concentration gradient from the feed side. The mass transport phenomena occur with convection with a velocity of average molecules, and diffusion occurs due to concentration differences in a fluid.

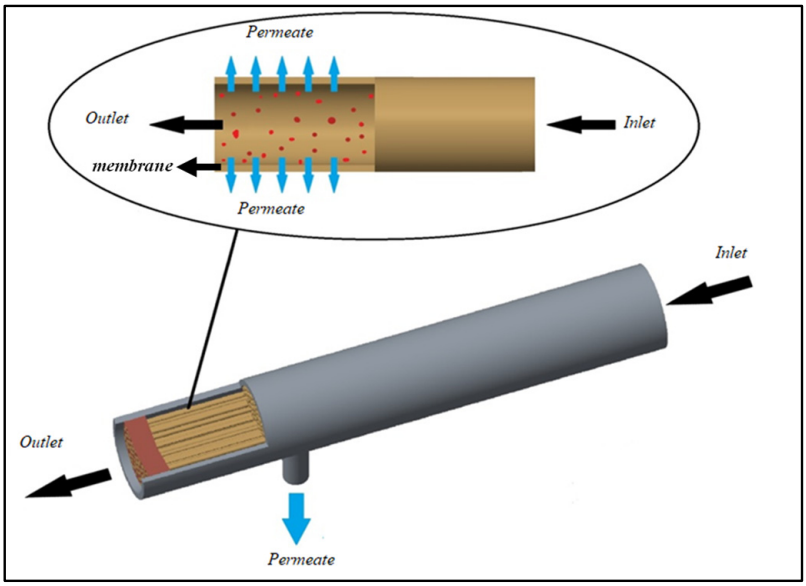

Figure 1. HFM module unit [40].

2.2.1. Convection and Diffusion Models

The mass transport equation contains both the convection and diffusion models. The mass transport equation is as follows:

$$\frac{\partial C_a}{\partial t} + v_x \frac{\partial C_a}{\partial x} + v_y \frac{\partial C_a}{\partial y} + v_z \frac{\partial C_a}{\partial z} = D_{AB} \left[\frac{\partial^2 C_a}{\partial x} + \frac{\partial^2 C_a}{\partial y} + \frac{\partial^2 C_a}{\partial z} \right] + R_a \quad (1)$$

The bulk velocity v (x, y, and z) is used for convective transport, and velocity is measured by combining two equations, mass balance and momentum equation. The mass balance equation represents a diffusion mechanism that deals with the diluted and solvent species on the feed side of the membrane. Operators show three directions of space variables in the x-, y-, and z-direction. Finally, the source term is on the right side of the equation, showing a chemical reaction that occurred in a process. The term "a" is defined as the concentration of gas on the feed side.

2.2.2. Diffusion

The transport of diluted species provides an environment for modeling mass transport in a chemical species. Here, the diluted species interface model is applied, showing all species in a diluted form. When a dilution model is applied, it shows that the properties of the solute are the same as a present solvent. Fick's Law also defines solution diffusion in a mixture. The transport of dilute species provides both convection and diffusion models for simulation in all dimensions.

$$N_a = -D_{\mathrm{AB}} \left[\frac{\partial^2 C_a}{\partial x} + \frac{\partial^2 C_a}{\partial y} + \frac{\partial^2 C_a}{\partial z} \right] \quad (2)$$

where diffusion is represented as D_{AB}.

2.2.3. Membrane Model

Diffusion is an essential mechanism occurring in mass transfer problems. It mainly focuses on the diffusion through membranes for certain chemical species. The system is considered to check the permeability of gases, where the feed side of gas in the fiber-bore side and permeate is passed through a membrane collected on the shell side. The unit of the membrane module demonstrates the membrane model.

The model equation for steady-state mass transfer is as follows:

$$D_{\mathrm{AB}} \left[\frac{\partial^2 C_a}{\partial x} + \frac{\partial^2 C_a}{\partial y} + \frac{\partial^2 C_a}{\partial z} \right] = 0 \quad (3)$$

The scalar product of concentration gradient C_a (mole/m^3) and D_{AB} diffusion coefficient of the diffusing species (m^2/s) shows a steady-state mass transfer equation. All boundaries considered isolating conditions.

$$D_{\mathrm{AB}} \left[\frac{\partial C_a}{\partial x} + \frac{\partial C_a}{\partial y} + \frac{\partial a}{\partial z} \right] = 0 \quad (4)$$

The boundary condition is considered as the fiber-bore side applied as an inlet that shows a concentration of component C_0 and the shell side considered as the reject side $C_{0,1}$.

Boundary conditions 1 and 2 are represented as

$$C_1 = C_0;\ C_2 = C_{0,1} \quad (5)$$

2.2.4. Flow through Membrane in HFM Module

The membrane flux is investigated through the membrane in terms of diffusion D with solubility S with inlet concentration C_0 and outlet concentration $C_{0,1}$.

$$N_a = \frac{D \cdot S}{\delta}(C_0 - C_{0,1}) \tag{6}$$

Term $\frac{D}{\delta}$ is determined as a barrier with corresponding thickness.

The concentration is defined in terms of partial pressure p_a and solubility s_a for component a through the membrane. The term a is defined as any gas component.

$$C = p_a \times s_a \tag{7}$$

The flux through the membrane is presented in terms of permeability and partial pressure:

$$N_a = \frac{\frac{P}{S}}{\delta}(pf \times s_a - ph \times s_a) \tag{8}$$

The pressure difference between both sides is used as a gradient for inlet pressure pf and permeate pressure ph. The ratio of their differences is called solubility for the binary mixture. This membrane model was applied to HFM membrane modules to find the flow profiles and flux of gases. The symbols of the equation were mentioned in the Appendix A.

2.3. Flowchart of Post-Processing Scheme

The numerical simulation schemes chart is represented in Figure 2.

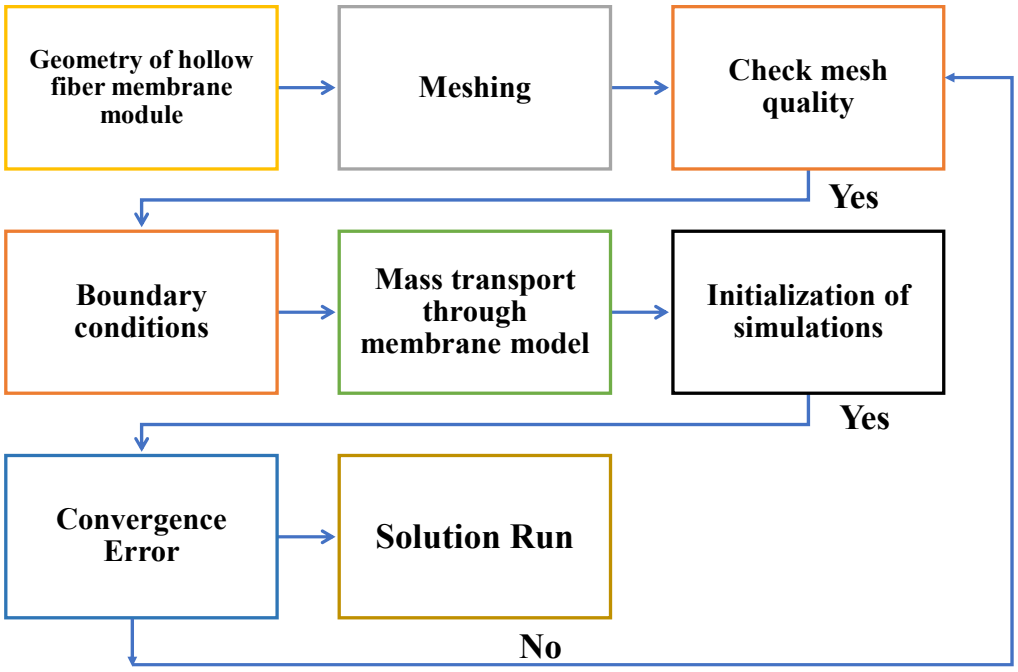

Figure 2. Post-processing flow diagram for CFD simulations.

2.4. Geometry

The sketches of geometries for HFM modules are shown in Figure 3.

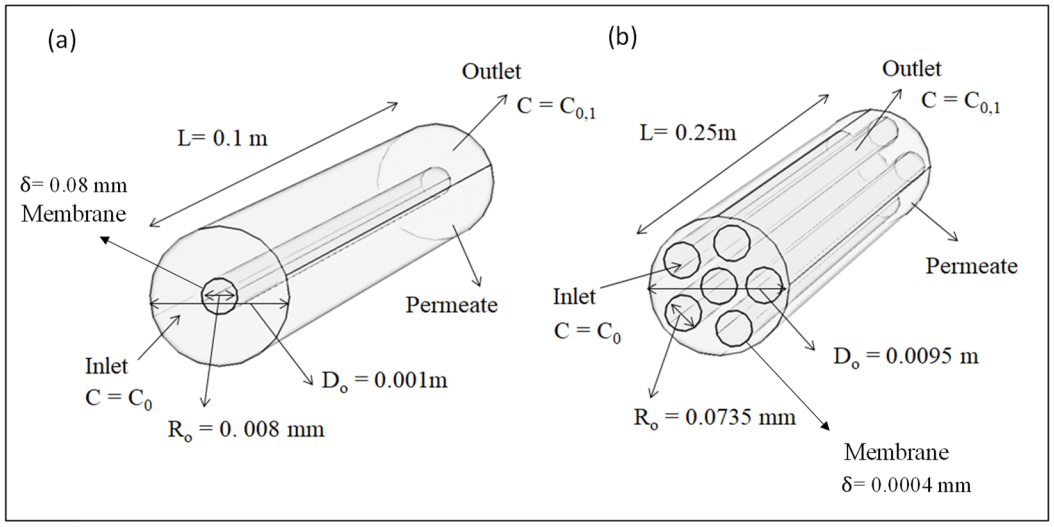

Figure 3. Schematic diagram of the single tube and HFM module. (**a**) Single hollow fiber case study for CO_2/CH_4 separation (**b**) Multiple hollow fiber membrane module for N_2/O_2 separation.

2.5. Meshing

The finite element method was used in the HFM module to solve the mass transport problem and meshing of the membrane module in COMSOL Multiphysics. The HFM complete mesh consisted of 13,191,478 domain elements, 2,281,754 boundary elements, and 223,387 edge elements, and degrees of freedom were solved at 1,364,033 (plus 864,222 internal DOFs). Solution time (Study 1): 230 s. (3 min, 50 s). In addition, one fiber tube consisting of 3,813,513 domain elements, 318,624 boundary elements, and 8988 edge elements and degrees of freedom was solved for 723,639 (plus 328,506 internal DOFs). The mesh for the membrane was generated using a triangular mesh structure. The results obtained from boundary layer mesh analysis are shown in Table 2. The resulting mesh is shown in Figure 4e. The analysis of the module mesh was observed, and the inlet region shows a higher density segment. Furthermore, membrane meshing is more critical in the CFD simulations because the inner membrane wall formed the concentration boundary layer. Therefore, membrane refinement along with membrane thickness are essential.

Table 2. Boundary layer mesh analysis.

Parameters	Total Elements
Solution time (Study 1)	625 s
Number of edge elements	33,311
Number of boundary elements	779,926
Number of elements	6,376,565
Minimum element quality	7.11×10^{-5}

For the boundary layer in the membrane, selecting wall thickness of the fiber as a porous surface is necessary. The representative mesh for the membrane was generated using a triangular mesh structure. The mesh analysis observes a higher density of elements in the feed region and near the interface region between the fluid and the porous medium. This refinement is based on the numerical study which considered inner wall thickness. The formation of the concentration boundary layer occurs with low thickness, confirming the significant concern with the mesh in this region.

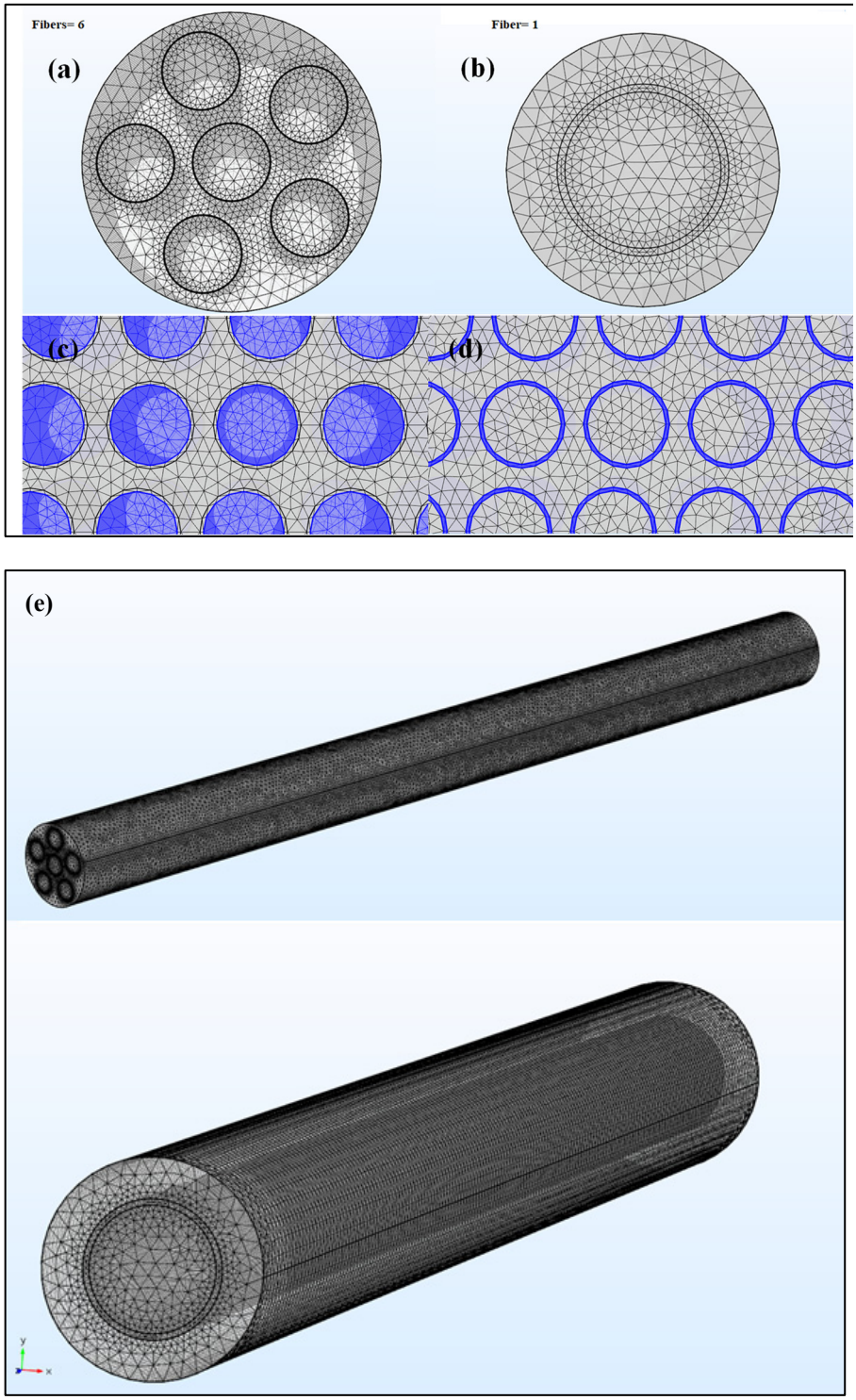

Figure 4. (**a**) Meshing of HFM membrane module for six fibers; (**b**) the meshing of single-tube HFM module; (**c**) fiber-lumen side meshing for inlet flow in the HFM module; (**d**) membrane thickness meshing; and (**e**) 3-D meshing of both single and six fiber HFM.

3. Results

This work was carried out using COMSOL Multiphysics software 5.2 version for the HFM module design using CFD. Furthermore, the effects of module length on the diffusive flux, total flux, and concentration variations were determined using CFD.

3.1. Air Separation

The HFM module simulations were performed for oxygen separation from air. The flow variations were obtained from O_2 gas on the shell side of the HFM module. The inlet gas enters the membrane module from the lumen side, and thus, a crossflow model is considered as the boundary condition. The boundary condition was applied for a high inlet concentration on the lumen side, C_0, and a low inlet concentration on the shell side, C_0. Figure 5a shows that the feed gas, O_2, permeates through membrane fibers, and a maximum purity of the N_2 was obtained on the shell side. The concentration between the fibers was changed due to high flux on the inlet side and increased gas purity in the permeate stream. Based on these results, it was concluded that permeation of O_2 occurred through the fiber. Figure 5b indicates that the concentration variation between two fibers is more important. The two-dimensional results verified that O_2 gas diffused through the membrane due to the concentration gradient, and a variation in gas was obtained in the membrane module's center. In addition, the difference between the fibers was negligible due to the compactness of the fibers, but the permeate shell showed maximum gas diffusion from the high inlet side to the outlet side.

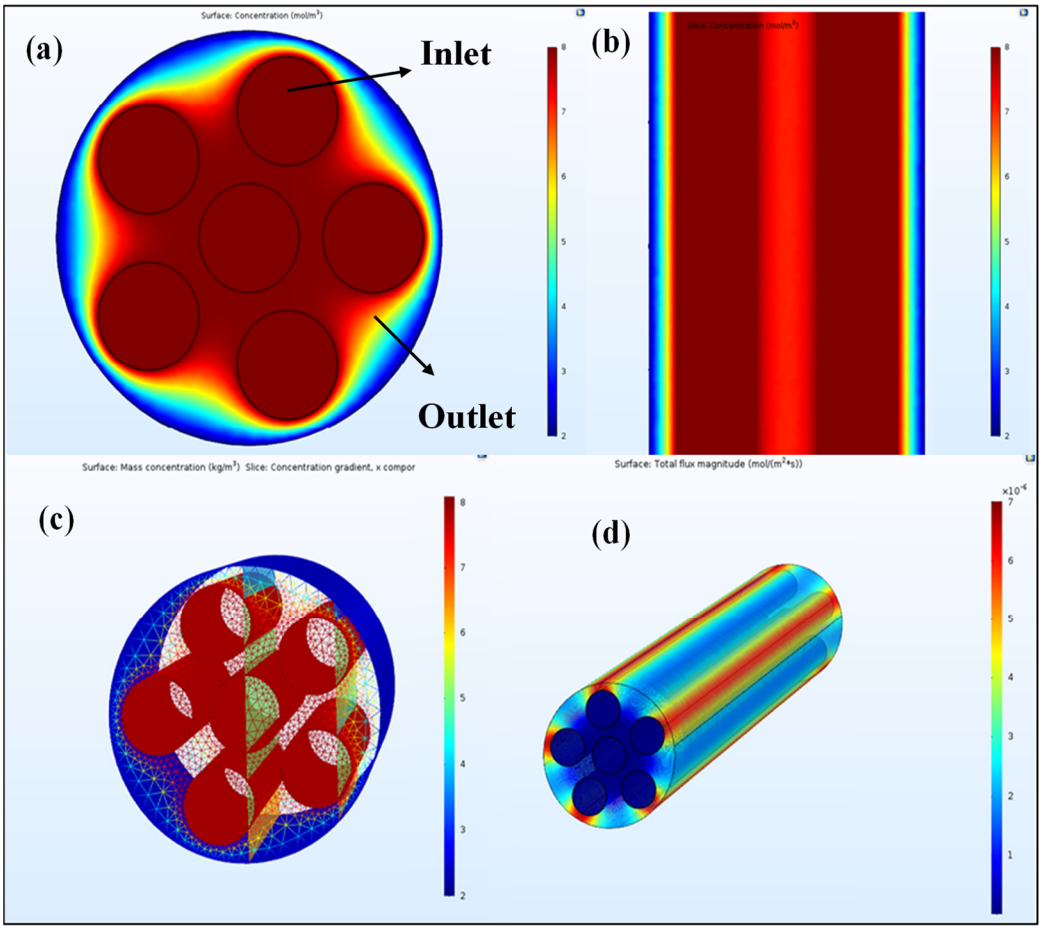

Figure 5. (**a**) Oxygen gas concentration in inlet and outlet side in HFM module; (**b**) 2-dimensional inlet oxygen concentration variation in the HFM module; (**c**) oxygen inlet variation as gradient high to low in the HFM module; (**d**) oxygen flux magnitude in HFM module.

The concentration gradient displayed in Figure 5c shows that the gas diffusion varied at different mesh points from the inlet to the permeate side. The red mesh points on the shell side show the maximum purity of O_2 gas on the permeate side. The different mesh points in the center show the different gas concentrations of O_2 purity. It was confirmed that the concentration gradient was present in the HFM module due to the partial pressure

of gases, and gas transported through the membrane with specific permeability. Figure 5d shows the diffusive flux magnitude variations in the HFM module for binary gas separation. Contours display a high flux variation on the shell side due to gas diffused from the inlet side to the permeate side. The results showed no pressure drop on the retentate side, and fluxes remained unchanged in the membrane center due to the diffusion of O_2 from the fiber side to the shell side.

3.2. Carbon Dioxide Separation

The HFM module geometry consists of a bundle of fibers in a single shell compacted together to form a large surface area, but in this case, the single fiber was used for gas separation. Figure 6a shows that the concentration of the inlet gas CO_2 changed on the feed side and permeate side. The gas entered from the lumen, and the crossflow model was considered for flow conditions. The fiber-bore side was considered as the inlet side boundary condition C_0 at one end, and another was considered the outlet boundary condition with the low concentration $C_{0,1}$. The thickness of the fiber shows as the membrane, which is a thin diffusion barrier. It was concluded that the contour expressing the CO_2 gas concentration variation always occurred from the feed side to permeate side.

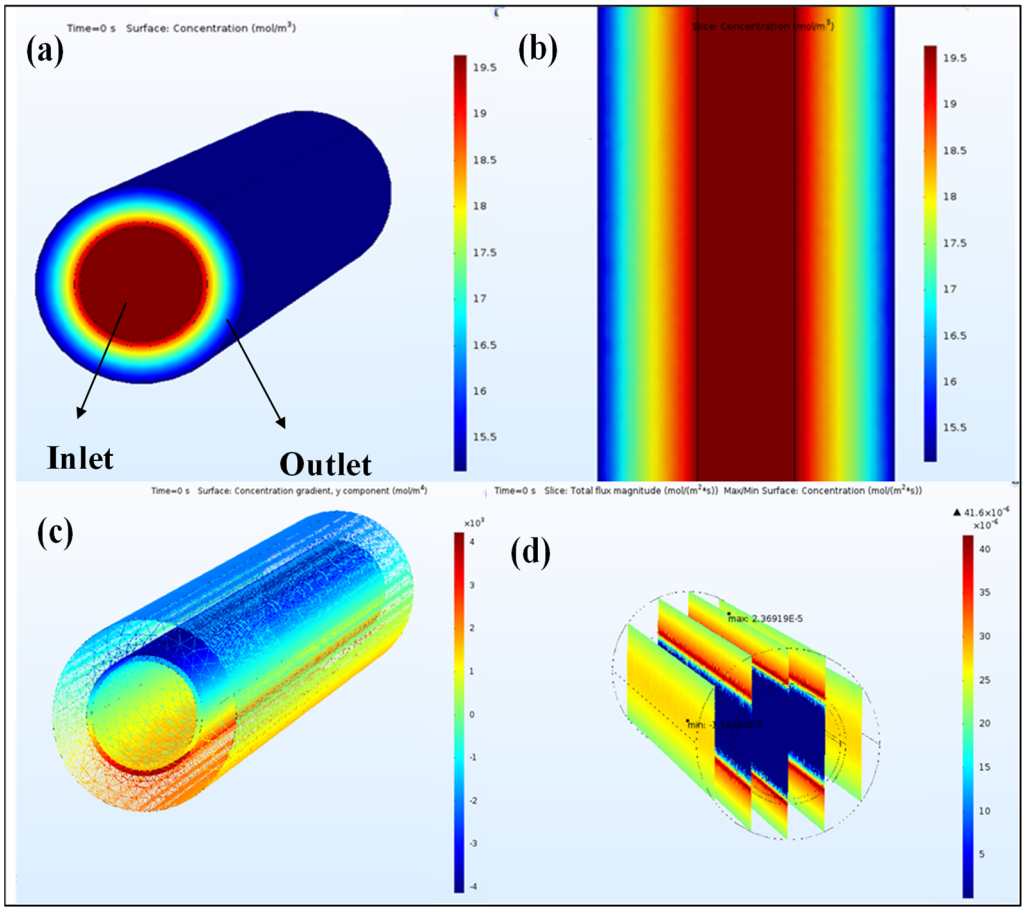

Figure 6. (**a**) Inlet gas CO_2 concentration in inlet and outlet sides in HFM module; (**b**) CO_2 2-dimensional gas variation model in HFM module; (**c**) CO_2 gas inlet variation as gradient high to low in HFM module; (**d**) CO_2 flux magnitude in HFM module.

Figure 6b shows the concentration of CO_2 in the two-dimensional model. From Figure 6b, the inlet gas variations from the inlet channel to the permeate collector can be observed. The maximum gas concentration at the fiber surface was higher because of the higher gas concentration transported through the membrane from the retentate. The results showed that gas diffused through the membrane at a higher permeation rate.

A concentration gradient was observed in the HFM module for CO_2. The different mesh points show that the inlet gas passes through the fiber side to the permeate side of the module, and the gradient below the fiber is higher due to the maximum gas diffusion through the membrane. The results showed that the gradient was present, and gas was diffused through the membrane. Figure 6d demonstrates the diffusive flux from the gradient applied from the lumen to the shell side. The flux was calculated with the given parameters of the membrane module. The flux magnitude variations describe binary gas separation in the HFM membrane module. Contours display a high flux variation on the shell side due to gas diffused from the inlet side to the permeate side. The results showed the zero pressure drop on the lumen side as the feed on the membrane, and fluxes remained unaffected.

4. Discussion

The HFM module performance was investigated using different parameters, such as fiber length (L), inlet pressure (pf), inlet concentration (xf), fiber bundle radius (Ro), and outer module diameter (Do).

Figure 7a shows the simulation of O_2/N_2 separation through the membrane. The results obtained from simulations show that the increment in the length of the fiber from 5 to 25 cm reduced the purity of O_2 from 15 to 10%, while the concentration of N_2 in the retentate stream was enhanced by 10%. The fiber length produced a large membrane area used for separation. The higher stage cut also caused more gas to permeate through the membrane because the extension in length gradually diluted the permeate stream with N_2; thus, O_2 possessed a lower quantity while the permeate possessed a higher quantity of N_2. Therefore, the purity of the permeate side was decreased. The oxygen depletion from the feed side to the permeate stream was less enriched, while a higher stage cut was achieved.

The concentration effect was investigated by changing the values of O_2 concentration in the feed while keeping other parameters constant. The feed concentration analysis shown in Figure 7b demonstrated that the concentrations of O_2 and N_2 were varied in the permeate and reject side, respectively. The results showed that the increment in the concentration of O_2 on the feed side provides a higher permeate rate in the stream. A further increment in O_2 concentration in the feed stream produced a higher concentration gradient, while the N_2 gradient was reduced. For the long fiber, lower O_2 and higher N_2 purities were obtained at all specified feed concentrations. O_2 purity in the permeate and N_2 in the retentate stream as a function of the mole fraction of O_2 in the feed are presented in Figure 7b.

Furthermore, the effect of pressure on the HFM was also investigated by changing the feed pressure from 5 to 25 bar. Interestingly, the increment in feed pressure provides different behavior for O_2 at the permeate stream and N_2 at the retentate stream. Figure 7c describes the effect of feed pressure on the concentration of O_2 and N_2 in the permeate and retentate streams. It was found that the increment in feed pressure provides a higher permeate concentration of O_2, while a further increment in feed pressure reduced the O_2 in the permeate. Increases in the feed pressure also produced an excessive mass transfer gradient for N_2, which transported through membrane and thus reduced the concentration of O_2 in the permeate stream. Furthermore, it was also observed that the maximum purity was achieved for a long fiber length with low feed pressure, mainly because of the larger membrane surface available in permeation.

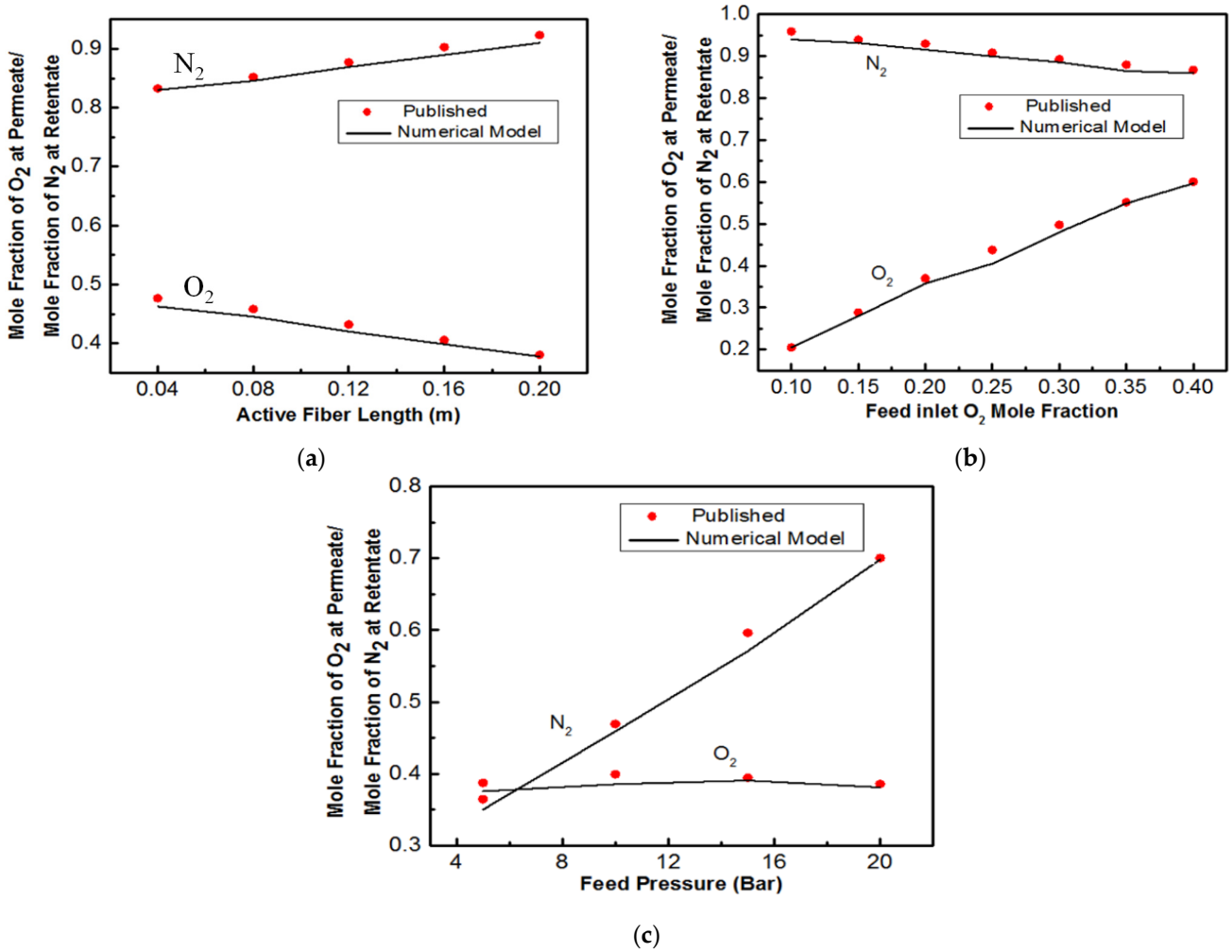

Figure 7. (**a**) O_2 and N_2 mole fraction variations with fiber length in HFM module; (**b**) mole fraction of O_2/N_2 with fiber length in permeate and reject sides in HFM module (Reprinted with permission from Ref. [36]. 2016, Seyed Saeid) [36]; (**c**) feed mole fraction of the O_2/N_2 in permeate and reject sides in HFM module (Reprinted with permission from Ref. [36]. 2016, Seyed Saeid) [36].

The increase in fiber length gives more losses of CH_4 because the increment in fiber length provides a higher surface area of the membrane. Therefore, higher permeation resulted in significant methane loss, as shown in Figure 8a. The CO_2 in the feed is a more permeable component with a more significant effect of a mole fraction of CO_2 on the permeate side. On the other hand, the negative quadratic impact of the CO_2 mole fraction significantly affects the feed side. Higher fiber length directly affects the purity of CO_2 and higher methane loss on the retentate side because of its lower concentration. The maximum purity of the CO_2 of 80% was obtained when the fiber length was short. From Figure 8b, results show that increasing the fiber length is not always favorable in that increased length caused a less driving force for overcoming resistance. For instance, the mole fraction of the more permeable component in the permeate stream decreased from 2% to 0.6% by increasing the length of fibers from 5 to 25 cm. The same trends were obtained to increase the fiber bundle radius, which showed more methane loss on the reject side. This decrease may be explained by the fact that maximum CO_2 purity was obtained when the fiber length was small or the number of fibers was at the minimum.

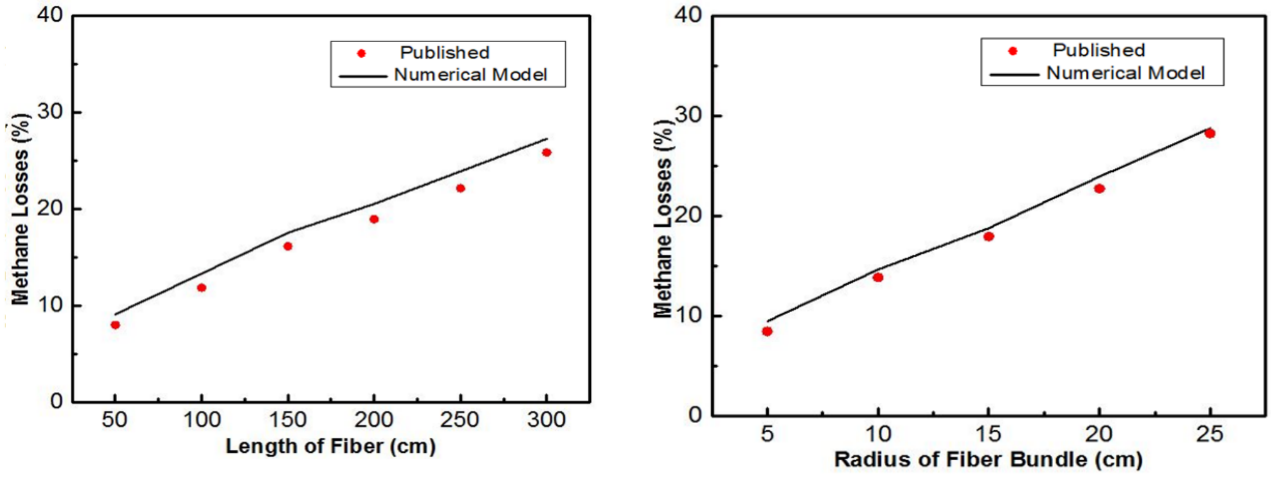

(**a**) (**b**)

Figure 8. (**a**) Effect of fiber radius on methane loss on the permeate side (Reprinted with permission from Ref. [37]. 2015, Faizan Ahmed) [37]; (**b**) fiber length effect on methane loss in HFM module (Reprinted with permission from Ref. [37]. 2015, Faizan Ahmed) [37].

5. Conclusions

The gas separation performance of an HFM unit was studied using the COMSOL Multiphysics Software. A CFD analysis for N_2/O_2 and CO_2/CH_4 separation was performed considering different parameters, such as fiber length (L), feed pressure (p_f), feed concentration (x_f), fiber bundle radius (R_o), and outer module diameter (D_o). Three-dimensional geometry was developed by using COMSOL geometry, and meshing was performed using triangular mesh. It was observed that an increment in fiber length reduced the oxygen purity because of the diluted permeate stream. The increment in feed concentration resulted in increasing the purity of the permeate. The HFM unit observed that increased feed pressure results in an increased pressure gradient, higher flux, more permeability, and higher permeate purity. Similarly, an increment in feed concentration increased the permeate mole fraction, facilitating the permeate stream and producing higher purities of O_2 (20% to 75%) and CO_2 (65% to 85%).

Author Contributions: Conceptualization, writing—review and editing, M.A.; methodology; validation; formal analysis; investigation; resources, data curation, writing—original draft preparation, S.Q.; visualization; supervision, A.H. All authors have read and agreed to the published version of the manuscript.

Funding: This research received no external funding.

Data Availability Statement: Data is unavailable due to privacy or ethical restrictions.

Conflicts of Interest: The authors declare no conflict of interest.

Appendix A

List of symbols

Acronyms

CFD	Computational fluid dynamics
HFM	Hollow fiber membrane
N_2	Nitrogen
O_2	Oxygen
CO_2	Carbon dioxide
CH_4	Methane

Greek Symbols	
x x	Co-ordinate
y y	Co-ordinate
z z	Co-ordinate
Vx	Velocity in x-direction
Vy	Velocity in y-direction
Vz	Velocity in z-direction
"∇"	Nabla operator
Latin symbols t time (s)	
Ra.	Rate of reaction (mol/m^3.s)
N	Molar flux (mol/.m^2. s)
D	Diffusion coefficient (m^2/s)
S	Solubility (mol/m^3.pa)
P	Permeance (mol/m^2.s.pa)
C	Concentration of component (mol/m^3)
P	Partial pressure
L	Module length (m)
Do	Module diameter (m)
Ro	Fiber bundle radius (m)
δ	Membrane thickness (m)
C	Gas species concentration (mol/m^3)
D_AB	Diffusivity coefficient (m^2/s)
C_0	Concentration of inlet (mol/m^3)
C_0,1	Concentration of outlet (mol/m^3)
P	Permeability of the gas (mol/m^2.s.pa)
S	Membrane solubility (mol/m^3.pa)
pf	Pressure of the inlet side (Pa)
ph	Pressure of the permeate side (Pa)
δ	Membrane thickness (m)
ΔC	Concentration gradient (mol/m^3)
Δp	Gradient of the partial pressure of gases (Pa/m)

References

1. Bernardo, P.; Drioli, E.; Golemme, G. Membrane Gas Separation: A Review/State of the Art. *Ind. Eng. Chem. Res.* **2009**, *48*, 4638–4663. [CrossRef]
2. Sanaeepur, H.; Amooghin, A.E.; Moghadassi, A. Modeling and Simulation for Membrane Gas Separation Processes. In *Modeling in Membranes and Membrane-Based Processes*; Scrivener Publishing LLC: Arak, Iran, 2020; pp. 201–235. [CrossRef]
3. Ardaneh, M.; Abolhasani, M.; Esmaeili, M. CFD modeling of two-stage H2 recovery process from ammonia purge stream by industrial hollow fiber membrane modules. *Int. J. Hydrogen Energy* **2019**, *44*, 4851–4867. [CrossRef]
4. Mousavian, S.; Faravar, P.; Zarei, Z.; Azimikia, R.; Monjezi, M.G.; Kianfar, E. Modeling and simulation absorption of CO_2 using hollow fiber membranes (HFM) with mono-ethanol amine with computational fluid dynamics. *J. Environ. Chem. Eng.* **2020**, *8*, 103946. [CrossRef]
5. Ghobadi, J.; Ramirez, D.; Khoramfar, S.; Kabir, M.; Jerman, R.; Saeed, M. Mathematical modeling of CO_2 separation using different diameter hollow fiber membranes. *Int. J. Greenh. Gas Control.* **2020**, *104*, 103204. [CrossRef]
6. Kundu, P.K.; Chakma, A.; Feng, X. Modelling of multicomponent gas separation with asymmetric hollow fibre membranes-methane enrichment from biogas. *Can. J. Chem. Eng.* **2012**, *91*, 1092–1102. [CrossRef]
7. Khanafer, K.; Assad, M.E.H. Mathematical Modeling of Fluid Flow Through a Hollow Fiber Water System Using Porous Medium Model. *Arab. J. Sci. Eng.* **2021**, *47*, 6049–6057. [CrossRef]
8. Chen, W.-H.; Lin, C.-H.; Lin, Y.-L. Flow-field design for improving hydrogen recovery in a palladium membrane tube. *J. Membr. Sci.* **2014**, *472*, 45–54. [CrossRef]
9. Jafari, M.; Rahimpour, E.; Rahimpour, M.R. Application of computational fluid dynamics technique in processes of gas membrane separation. In *Current Trends and Future Developments on (Bio-) Membranes*; Elsevier: Amsterdam, The Netherlands, 2021; pp. 269–288. [CrossRef]
10. Markova, S.Y.; Dukhov, A.V.; Pelzer, M.; Shalygin, M.G.; Vad, T.; Gries, T.; Teplyakov, V.V. Designing 3D Membrane Modules for Gas Separation Based on Hollow Fibers from Poly(4-methyl-1-pentene). *Membranes* **2021**, *12*, 36. [CrossRef]
11. Bernardo, P.; Clarizia, G. 30 years of membrane technology for gas separation. *Chem. Eng.* **2013**, *32*, 1999–2004.

12. Liu, Y.; Cui, X.; Yan, W.; Su, J.; Duan, F.; Jin, L. Analysis of pressure-driven water vapor separation in hollow fiber composite membrane for air dehumidification. *Sep. Purif. Technol.* **2020**, *251*, 117334. [CrossRef]
13. Hashim, S.; Mohamed, A.R.; Bhatia, S. Oxygen separation from air using ceramic-based membrane technology for sustainable fuel production and power generation. Renew. Sustain. *Energy Rev.* **2011**, *15*, 1284–1293. [CrossRef]
14. Shamsabadi, A.A.; Kargari, A.; Farshadpour, F.; Laki, S. Mathematical modeling of CO_2/CH_4 separation by hollow fiber membrane module using finite difference method. *J. Membr. Sep. Technol.* **2012**, *1*, 19–29.
15. Li, X.; Younas, M.; Rezakazemi, M.; Ly, Q.V.; Li, J. A review on hollow fiber membrane module towards high separation efficiency: Process modeling in fouling perspective. *Chin. Chem. Lett.* **2021**, *33*, 3594–3602. [CrossRef]
16. Cancilla, N.; Gurreri, L.; Marotta, G.; Ciofalo, M.; Cipollina, A.; Tamburini, A.; Micale, G. Performance Comparison of Alternative Hollow-Fiber Modules for Hemodialysis by Means of a CFD-Based Model. *Membranes* **2022**, *12*, 118. [CrossRef]
17. Feng, B.; Song, J.; Wang, Z.; Dewangan, N.; Kawi, S.; Tan, X. CFD modeling of the perovskite hollow fiber membrane modules for oxygen separation. *Chem. Eng. Sci.* **2020**, *230*, 116214. [CrossRef]
18. Lock, S.; Lau, K.; Ahmad, F.; Shariff, A. Modeling, simulation and economic analysis of CO_2 capture from natural gas using cocurrent, countercurrent and radial crossflow hollow fiber membrane. *Int. J. Greenh. Gas Control.* **2015**, *36*, 114–134. [CrossRef]
19. Cancilla, N.; Gurreri, L.; Marotta, G.; Ciofalo, M.; Cipollina, A.; Tamburini, A.; Micale, G. A porous media CFD model for the simulation of hemodialysis in hollow fiber membrane modules. *J. Membr. Sci.* **2022**, *646*, 120219. [CrossRef]
20. Ahsan, M.; Hussain, A. Computational fluid dynamics (CFD) modeling of heat transfer in a polymeric membrane using finite volume method. *J. Therm. Sci.* **2016**, *25*, 564–570. [CrossRef]
21. Ahsan, M.; Hussain, A. A computational fluid dynamics (CFD) approach for the modeling of flux in a polymeric membrane using finite volume method. *Mech. Ind.* **2017**, *18*, 406. [CrossRef]
22. Ghidossi, R.; Veyret, D.; Moulin, P. Computational fluid dynamics applied to membranes: State of the art and opportunities. *Chem. Eng. Process.—Process. Intensif.* **2006**, *45*, 437–454. [CrossRef]
23. Foo, K.; Liang, Y.; Goh, P.; Ahmad, A.; Wang, D.; Fletcher, D. Comparison of analytical film theory and a numerical model for predicting concentration polarisation in membrane gas separation. Chem. *Eng. Res. Des.* **2022**, *185*, 281–290. [CrossRef]
24. Dash, S.; Mohanty, S. Separation of lanthanum and neodymium in a hollow fiber supported liquid membrane: CFD modelling and experimental validation. *Miner. Eng.* **2022**, *180*, 107472. [CrossRef]
25. Marcos, B.; Moresoli, C.; Skorepova, J.; Vaughan, B. CFD modeling of a transient hollow fiber ultrafiltration system for protein concentration. *J. Membr. Sci.* **2009**, *337*, 136–144. [CrossRef]
26. Ranade, V.V.; Kumar, A. Fluid dynamics of spacer filled rectangular and curvilinear channels. *J. Membr. Sci.* **2006**, *271*, 1–15. [CrossRef]
27. Lukitsch, B.; Ecker, P.; Elenkov, M.; Janeczek, C.; Haddadi, B.; Jordan, C.; Krenn, C.; Ullrich, R.; Gfoehler, M.; Harasek, M. Computation of Global and Local Mass Transfer in Hollow Fiber Membrane Modules. *Sustainability* **2020**, *12*, 2207. [CrossRef]
28. Haghshenasfard, M.; Moheb, A.; Ansaripour, M. Application of computational fluid dynamics technique in membrane contactor systems. In *Current Trends and Future Developments on (Bio-) Membranes*; Elsevier: Amsterdam, The Netherlands, 2021; pp. 289–310. [CrossRef]
29. Ng, E.; Lau, K.; Lau, W.; Ahmad, F. Holistic review on the recent development in mathematical modelling and process simulation of hollow fiber membrane contactor for gas separation process. *J. Ind. Eng. Chem.* **2021**, *104*, 231–257. [CrossRef]
30. Tahmasbi, D.; Hossainpour, S.; Babaluo, A.A.; Rezakazemi, M.; Souq, S.S.M.N.; Younas, M. Hydrogen separation from synthesis gas using silica membrane: CFD simulation. *Int. J. Hydrogen Energy* **2020**, *45*, 19381–19390. [CrossRef]
31. Coroneo, M.; Montante, G.; Baschetti, M.G.; Paglianti, A. CFD modelling of inorganic membrane modules for gas mixture separation. *Chem. Eng. Sci.* **2009**, *64*, 1085–1094. [CrossRef]
32. Chen, W.-H.; Syu, W.-Z.; Hung, C.-I.; Lin, Y.-L.; Yang, C.-C. A numerical approach of conjugate hydrogen permeation and polarization in a Pd membrane tube. *Int. J. Hydrogen Energy* **2012**, *37*, 12666–12679. [CrossRef]
33. Qi, R.; Henson, M. Optimization-based design of spiral-wound membrane systems for CO2/CH4 separations. *Sep. Purif. Technol.* **1998**, *13*, 209–225. [CrossRef]
34. Gholami, G.; Soleimani, M.; Ravanchi, M.T. Mathematical Modeling of Gas Separation Process with Flat Carbon Membrane. *J. Membr. Sci. Res.* **2015**, *1*, 90–95. [CrossRef]
35. Kundu, P.K.; Chakma, A.; Feng, X. Simulation of binary gas separation with asymmetric hollow fibre membranes and case studies of air separation. *Can. J. Chem. Eng.* **2011**, *90*, 1253–1268. [CrossRef]
36. Hosseini, S.S.; Dehkordi, J.A.; Kundu, P.K. Gas permeation and separation in asymmetric hollow fiber membrane permeators: Mathematical modeling, sensitivity analysis and optimization. *Korean J. Chem. Eng.* **2016**, *33*, 3085–3101. [CrossRef]
37. Ahmad, F.; Lau, K.; Lock, S.; Rafiq, S.; Khan, A.U.; Lee, M. Hollow fiber membrane model for gas separation: Process simulation, experimental validation and module characteristics study. *J. Ind. Eng. Chem.* **2015**, *21*, 1246–1257. [CrossRef]
38. Katoh, T.; Tokumura, M.; Yoshikawa, H.; Kawase, Y. Dynamic simulation of multicomponent gas separation by hollow-fiber membrane module: Nonideal mixing flows in permeate and residue sides using the tanks-in-series model. *Sep. Purif. Technol.* **2011**, *76*, 362–372. [CrossRef]

39. Foo, K.; Liang, Y.; Goh, P.; Fletcher, D. Computational fluid dynamics simulations of membrane gas separation: Overview, challenges and future perspectives. *Chem. Eng. Res. Des.* **2023**, *191*, 127–140. [CrossRef]
40. McKeen, L.W. Markets and Applications for Films, Containers, and Membranes. *Permeabil. Prop. Plast. Elastomers* **2012**, *4*, 59–75. [CrossRef]